Rearrangement of the Distal Pocket Accompanying E7 His → Gln Substitution in Elephant Carbonmonoxy- and Oxymyoglobin: ^{1}H NMR Identification of a New Aromatic Residue in the Heme Pocket†

Liping P. Yu and Gerd N. La Mar*

Department of Chemistry, University of California, Davis, California 95616

Hiroshi Mizukami

Department of Biological Sciences, Wayne State University, Detroit, Michigan 48202

Received August 17, 1989; Revised Manuscript Received November 1, 1989

ABSTRACT: Two-dimensional ^{1}H NMR methods have been used to assign side-chain resonances for the residues in the distal heme pocket of elephant carbonmonoxymyoglobin (MbCO) and oxymyoglobin (MbO_2). It is shown that, while the other residues in the heme pocket are minimally perturbed, the Phe CD4 residue in elephant MbCO and MbO_2 resonates considerbly upfield compared to the corresponding residue in sperm whale MbCO. The new NOE connectivities to Val E11 and heme-induced ring current calculations indicate that Phe CD4 has been inserted into the distal heme pocket by reorienting the aromatic side chain and moving the CD corner closer to the heme. The $C_\zeta H$ proton of the Phe CD4 was found to move toward the iron of the heme by ~4 Å relative to the position in sperm whale MbCO, requiring minimally a 3-Å movement of the CD helical backbone. The significantly altered distal conformation in elephant myoglobin, rather than the single distal E7 substitution, forms a plausible basis for its altered functional properties of lower autoxidation rate, higher redox potential, and increased affinity for CO ligand. These results demonstrate that one-to-one interpretation of amino acid residue substitution (E7 His → Gln) is oversimplified and that conformational changes of substituted proteins which are not readily predicted have to be considered for interpretation of their functional properties.

The distal histidine residue (E7) in the conservative heme pocket of myoglobin, Mb,[1] and hemoglobin, Hb, has been assigned an important role in modulating the reactivity of the iron center (Satterlee et al., 1978; Case & Karplus, 1979; Baldwin, 1980; Phillips, 1980; Cutnell et al., 1981; Hanson & Schoenborn, 1981; Lavalette et al., 1984; Kuriyan et al., 1986; Olson et al., 1988; Perutz, 1989). The influence of the specific distal residues on the physical and functional properties of Mbs and Hbs has been studied for both natural genetic variants and mutants, such as elephant Mb (Romero-Herrera et al., 1981), shark Mb (Suzuki, 1987), human Hb (Tucker et al., 1978), *Aplysia* Mb (Peyton et al., 1989), liver fluke Hb (Di Iorio et al., 1985), *Chironomus* Hbs (Gersonde et al., 1987), and *Glycera* Hbs (Cooke et al., 1987), and more recently for recombinant mutants of sperm whale Mb and human Mb and Hb (Nagai et al., 1987; Olson et al., 1988; Springer et al., 1989; Lambright et al., 1989; Varadarajan et al., 1989). The ability to attribute these different properties of mutants to the distal residues implies that the invariant backbone in the heme pocket is conserved.

Sperm whale Mb has been extensively studied by a variety of methods and presently is the optimal reference protein for studying Mb mutants. Molecular dynamics simulations of sperm whale Mb show that there are large ground-state structural variations by loop displacement and helix orientation and that the range of predicted structural variations is similar to that found in the X-ray structures of different O_2 binding hemoproteins (Elber & Karplus, 1987). We are interested here in the case of the substitution E7 His → Gln, which occurs in elephant Mb (Dene et al., 1980), shark Mb (Suzuki, 1987; Suzuki & Furukohri, 1988; Suzuki et al., 1988), opossum Hb α-subunit (Sharma et al., 1982), hagfish Hb (Liljeqvist et al., 1982), and clam Hb (Suzuki et al., 1989). While the sequence homology of the other E7-substituted Mbs is very low to the reference sperm whale Mb protein, elephant Mb is an exceptional case with high homology to the reference protein. The amino acid sequence of elephant Mb was established from the overlapping enzymic peptides and by dansyl-Edman degradation (Dene et al., 1980) and shown to have a total of 28 substitutions (out of 153), among which a majority of them are located on the surface of the protein and only two (E7 His → Gln and CD3 Arg → Lys) are in the heme pocket. The CD3 Arg → Lys substitution is more common among Mbs from mammalian species such as human, horse, and dog. Elephant Mb is of considerable interest because it has very unusual properties, such as a significantly lower autoxidation rate (Romero-Herrera et al., 1981), a higher redox potential (Bartnicki et al., 1983), and selectively perturbed ligand binding rates (Romero-Herrera et al., 1981; Sharma et al., 1987). Since elephant Mb is often used as a model for point mutant studies (Magde et al., 1985; Li & Spiro, 1988) and some of the properties of elephant Mb are not common in all the other E7 Gln substituted proteins (Suzuki, 1987), the following questions arise: Are these altered properties due to

† This work was supported by Grant HL16087 from the National Institutes of Health.

[1] Abbreviations: Mb, myoglobin; Hb, hemoglobin; MbCO, carbonmonoxymyoglobin; MbO_2, oxymyoglobin; metMbCN, metcyanomyoglobin; metMb, metaquomyoglobin; RCT, relayed coherence transfer; DQF-COSY, double quantum filtered correlated spectroscopy; NOE, nuclear Overhauser effect; NOESY, nuclear Overhauser effect spectroscopy; DSS, 2,2-dimethyl-2-silapentane-5-sulfonate; ppm, parts per million.

0006-2960/90/0429-2578$02.50/0

the localized E7 His → Gln substitution or to significant perturbations of the ground-state structure? If they are due to the latter, is this perturbed ground state within the limits obtained from the dynamics simulation?

Resonance Raman studies of elephant Mb have been interpreted in terms of increased steric hindrance of the Fe–C–O moiety (Kerr et al., 1985). The NMR spectral features of elephant metMbCN are known to be very similar to those of sperm whale metMbCN (Krishnamoorthi et al., 1984b). However, there are more hyperfine-shifted downfield signals in elephant than sperm whale metMbCN upon accounting for the E7 substitution (Emerson, 1989). These strongly shifted signals and their dipolar connectivities and signal intensity pattern suggest insertion of an aromatic residue into the heme pocket (Emerson, 1989). For such an insertion, there must be some conformational rearrangement in the heme pocket as a result of E7 substitution in the metcyano form. Since it is known from the X-ray structural studies of *Chironomus* Hb that a distal residue exists in a unique orientation solely in the metcyano form (Steigemann & Weber, 1979), the logical questions that follow are: (1) Does the new residue observed in elephant metMbCN also occur in the physiologically relevant MbCO and MbO_2 forms? (2) What is the identity of this residue? (3) What are the structural consequences for the other conserved residues in the heme pocket? (4) Does the altered conformation form a more plausible basis than the point E7 substitution alone for the interpretation of the altered properties of elephant Mb?

Two-dimensional NMR spectroscopy provides particularly sensitive techniques for solution structure determination. In the diamagnetic complexes of interest, the position of distal residues can be inferred from the very large ring current shifts due to the heme and the localized conformation from the dipolar connectivities to the neighboring residues. In this paper, we carry out structural characterization of heme pocket residues with particular emphasis on the aromatic side chains in the distal pocket and demonstrate clearly the Phe CD4 insertion into the heme pocket in both elephant MbCO and MbO_2 complexes. This perturbed structure suggests that the different kinetic and functional properties of elephant Mb are not a result of simply replacing distal His with Gln but due to dramatic rearrangement of the CD corner (possibly including the E helix).

Experimental Procedures

Myoglobin from Asian elephant was isolated and purified as described earlier (Dene et al., 1980). The carbon monoxide complex of this protein was prepared by passing CO gas through 4 mM deoxymyoglobin in 99.9% ^2H_2O. The final sample contains 0.2 M NaCl and has a pH value adjusted to 8.7 with 0.2 M solutions of NaO^2H or ^2HCl. The MbO_2 sample was prepared by exchanging CO for O_2 of the MbCO sample in 66 mM phosphate buffer, pH 8.6, on iced water under strong light by flushing the pure O_2 gas over the sample for 2 h. The pH was measured in a NMR tube by an Ingold microcombination electrode and was uncorrected for the isotope effect.

NMR spectra were recorded at 30 °C for the MbCO sample and at 22 °C for the MbO_2 sample on a Nicolet NT-360 FTNMR spectrometer. Phase-sensitive NOESY (States et al., 1982), DQF-COSY (Edwards & Bax, 1986; Muller et al., 1986), and RCT (Wagner, 1983; Eich et al., 1982) employed the method described by States et al. (1982) to provide quadrature detection in the t_1 dimension. Magnitude-mode double quantum spectra were obtained with the pulse sequence t_o–$\pi/2$–τ–π–τ–$\pi/2$–t_1–$3\pi/4$–t_2, as described by Boyd et al. (1983). RCT experiments with the pulse sequence t_o–$\pi/2$–t_1–$\pi/2$–τ–π–τ–$\pi/2$–t_2 used the phase cycling of Wagner (1983). Solvent suppression, when required, was achieved by direct saturation in the relaxation delay period.

Typically, 256 scans were accumulated for each value of t_1, and 150 t_1 values (~29 ms) for phase-sensitive pure absorption 2D spectra and 300 t_1 (~58 ms) values for the double quantum spectra were recorded with free induction decays (FID) of 2048 and 1024 complex data points, respectively. The sweep width used was 5208 Hz. The 90° pulse width was 6.5 μs. Four dummy scans were used for each FID, and a recycle delay of 1.6 s including acquisition was employed. The 2D data were processed on a μ-Vax II computer with a Fortran program written by Dr. Dennis Hare. The time domain data were normally multiplied by a sine bell window function with phase shifts of 30° in the t_1 and t_2 dimensions and were zero-filled to obtain 1K × 1K real data points. Chemical shifts for all the spectra were referenced to 2,2-dimethyl-2-silapentane-5-sulfonate (DSS) through the residual water resonance.

Results

Heme Resonances. The two vinyl groups of the heme in MbCO can be identified from the DQF-COSY map (Figure 1A). The H_αs are located in the low-field region because of ring current shifts and are coupled to the H_{β_t}s and H_{β_c}s. Therefore, for one vinyl group, the H_α is found at 8.45 ppm, and the H_βs are at 5.78 and 5.69 ppm. For the other vinyl group, the H_α is found at 8.63 ppm, and the H_βs are at 6.53 and 6.29 ppm. The distinction between H_{β_t} and H_{β_c} can be made clearly on the basis of the J coupling constant and NOE intensity differences between the H_α and the H_{β_t} and H_{β_c}. The intensity of cross peaks between vinyl H_α and H_{β_c} is much stronger in the NOESY map (Figure 2) because of the shorter distance between them and much weaker in the DQF-COSY map (Figure 1A) because of the smaller cis than trans J coupling.

The heme methyl and meso-H resonances can be identified from the 2D NOESY map (not shown) on the basis of the structure of the heme (**1**). The meso-Hs are expected to

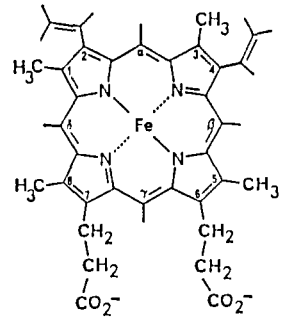

1

resonate at very low field because of ring current shifts. The α meso-H shows NOE connectivity to 3-CH_3 and 2-vinyl H_α, the β meso-H to 5-CH_3 and 4-vinyl H_α, and the δ meso-H to 1-CH_3 and 8-CH_3. The distinction between 2- and 4-vinyl groups and between 1-CH_3 and 8-CH_3 was made by observing the NOE connectivity between the 2-vinyl H_{β_t} and the 1-CH_3 group (not shown). The remaining low-field peak at 9.94 ppm is then assigned to γ meso-H. The assignments of heme ^1H resonances are summarized in Table I.

NOESY cross peaks are observed between the α meso-H and 2-vinyl H_α and H_{β_c} and between the β meso-H and 4-vinyl H_α and H_{β_c} (Figure 3). This observation agrees with the orientation of the vinyl groups with respect to other heme groups, as found in the crystal structure of sperm whale MbCO

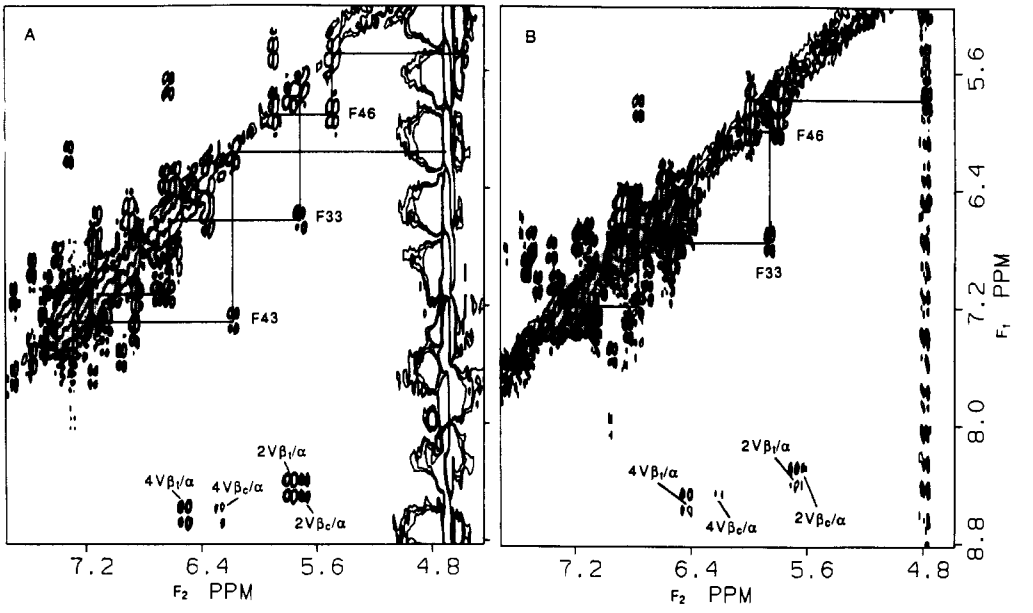

FIGURE 1: Aromatic region of the phase-sensitive DQF-COSY spectra of elephant MbCO at 30 °C (A) and MbO_2 at 22 °C (B). The assignments are shown with the one-letter code for the amino acid residues. The solid lines indicate the connectivities for the spin systems of the Phe aromatic rings. The residual water resonance is partially saturated in the experiment. The heme 2-vinyl group is labeled as 2V and the heme 4-vinyl group as 4V.

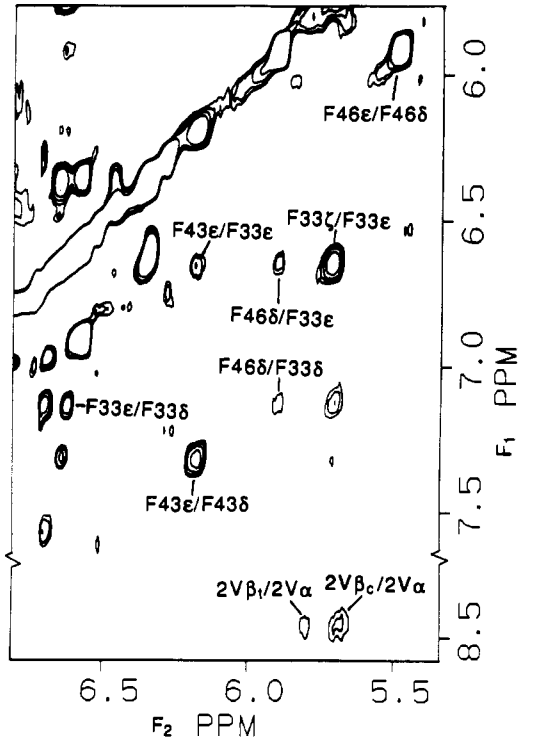

FIGURE 2: Aromatic region of the phase-sensitive NOESY spectrum of elephant MbCO. The mixing time τ_m = 250 ms. The heme 2-vinyl group is labeled as 2V. The other assignments are shown with the one-letter code for the amino acid residues.

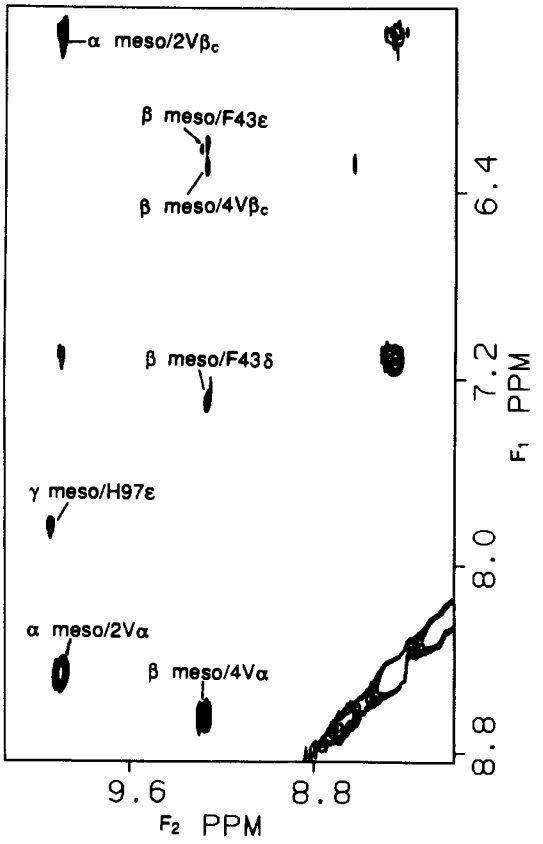

FIGURE 3: Aromatic region of the phase-sensitive NOESY spectrum of elephant MbCO. The mixing time τ_m = 250 ms. The heme 2-vinyl group is labeled as 2V and the heme 4-vinyl group as 4V. The other assignments are shown with the one-letter code for the amino acid residues and with the standard numbering for the heme.

(Kuriyan et al., 1986). The assigned vinyl, methyl, and α, β, and δ meso-Hs in elephant MbCO have very similar chemical shifts as compared with those in sperm whale MbCO (Mabbutt & Wright, 1985; Dalvit & Wright, 1987). The γ meso-H, however, is shifted upfield by 0.21 ppm, reflecting the distal substitution E7 His → Gln in elephant Mb. As in sperm whale MbCO, a strong NOESY peak between a proton at 7.83 ppm and the γ meso-H in elephant MbCO (Figure 3) is observed and assigned to the His 97 (FG3) imidazole ring proton ($C_\epsilon H$) which lies above the pyrrole III on the proximal side and close to the γ meso-H.

Upfield Resonances. There are two methyl peaks in the far-upfield region which must be due to the aliphatic residues located above or below the heme and close to the heme iron center. The far-upfield methyl at −1.98 ppm arises from a Val residue with chemical shifts at −1.98, −0.02, 1.10, and 3.27 ppm for the γ_2 CH_3, γ_1 CH_3, β CH, and α CH, respectively, as clearly identified from the DQF-COSY map (Figure 4) and

Table I: Assignments of ^1H NMR Resonances in Elephant MbCO and MbO_2

residues	chemical shifts (ppm)[a]	
	MbCO	MbO_2
heme meso	α 9.89, β 9.26, γ 9.94, δ 9.80	α 9.37, β 9.11, γ 9.47, δ 9.92
heme methyl	1-CH_3 3.68, 3-CH_3 3.78	1-CH_3 3.77, 3-CH_3 3.51
	5-CH_3 2.59, 8-CH_3 3.56	5-CH_3 2.59, 8-CH_3 3.56
heme 2-vinyl	α 8.45, β_t 5.78, β_c 5.69	α 8.34 β_t 5.69, β_c 5.61
heme 4-vinyl	α 8.63, β_t 6.53, β_c 6.29	α 8.52, β_t 6.44, β_c 6.20
Leu 29 (B10)	γ 0.68, δ_2 0.35, δ_1 −0.83	γ 0.70, δ_2 0.38, δ_1 −0.74
Phe^Y 33 (B14)	C_δHs 7.13, C_ϵHs 6.62, C_ζH 5.71	C_δHs 7.18, C_ϵHs 6.76, C_ζH 5.85
Phe^Z 43 (CD1)	C_δHs 7.31, C_ϵHs 6.18, C_ζH 4.75	*b*
Phe^X 46 (CD4)	C_δHs 5.91, C_ϵHs 5.49, C_ζH 4.59	C_δHs 5.99, C_ϵHs 5.79, C_ζH, 4.77
Val 68 (E11)	α 3.27, β 1.10, γ_1 −0.02, γ_2 −1.98	α 2.99, β 0.85, γ_1 −0.38, γ_2 −2.61
His 97 (FG3)	C_ϵH 7.83	C_ϵH 7.72

[a] In ^2H_2O solution at 30 °C for MbCO and at 22 °C for MbO_2. [b] Not resolved because of the line broadening resulting from the slow reorientation of the aromatic ring.

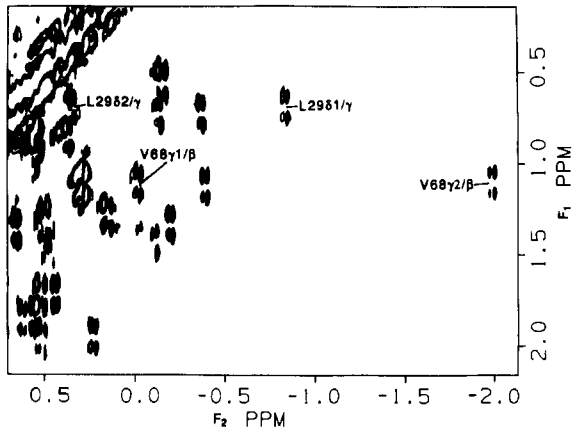

FIGURE 4: Upfield region of the phase-sensitive DQF-COSY spectrum of elephant MbCO. The assignments are shown with the one-letter code for the amino acid residues.

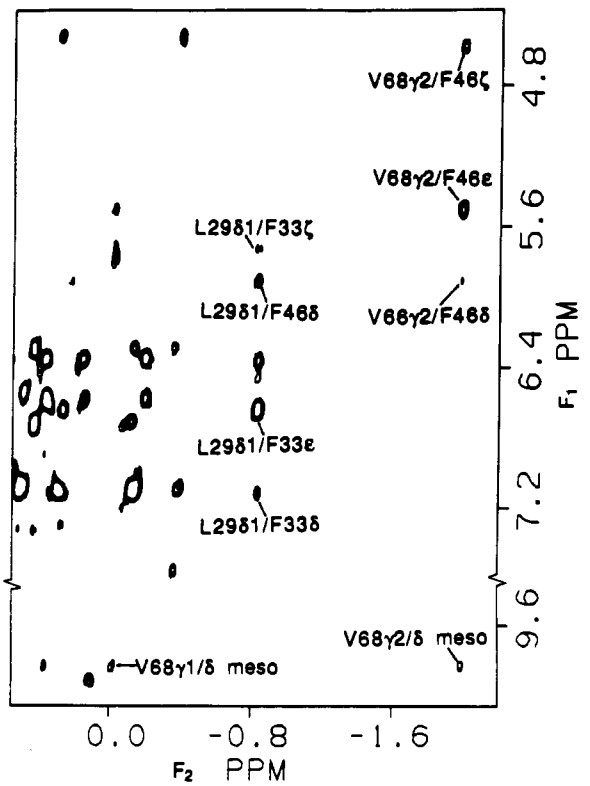

FIGURE 5: Region of the phase-sensitive NOESY spectrum of elephant MbCO, showing the NOE connectivities of Phe CD4 and Phe B14 to Val E11 and Leu B10. The mixing time τ_m = 250 ms. The assignments are shown with the one-letter code for the amino acid residues and with the standard numbering for the heme.

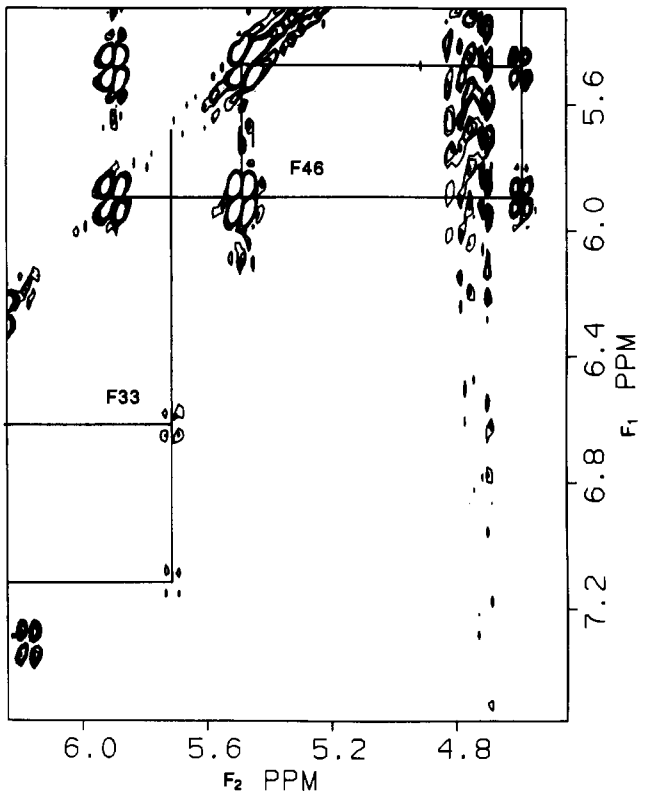

FIGURE 6: Aromatic region of the phase-sensitive relayed coherence transfer (RCT) spectrum of elephant MbCO, acquired with 2τ = 60 ms. The assignments are shown with the one-letter code for the amino acid residues. The t_1 ridge of the residual water resonance is seen at 4.70 ppm. The residual water resonance was partially saturated in the experiment.

RCT map (not shown). The observed NOE connectivities between the heme δ meso-H and the γ_2 CH_3 and γ_1 CH_3 (Figure 5) and α CH (not shown) of this Val residue are the same as those found in sperm whale MbCO for Val E11 with similar chemical shifts (Dalvit & Wright, 1987) and therefore unambiguously assign this spin system to Val 68 (E11). The other upfield methyl at −0.83 ppm is from a $-CH(CH_3)_2$ group as identified from the DQF-COSY map (Figure 4) and is located on the distal side as clearly inferred from the NOE connectivities (see below). Hence, it must originate from Leu 29 (B10). The chemical shifts for Leu B10 are −0.83, 0.35, and 0.68 ppm for the δ_1 CH_3, δ_2 CH_3, and γ CH, respectively, which are similar to those in sperm whale MbCO (Dalvit & Wright, 1987).

Phe Residues in the Heme Pocket. Three Phe aromatic ring spin systems can be identified clearly with a variety of conventional 2D NMR techniques. Figure 1A shows one Phe spin

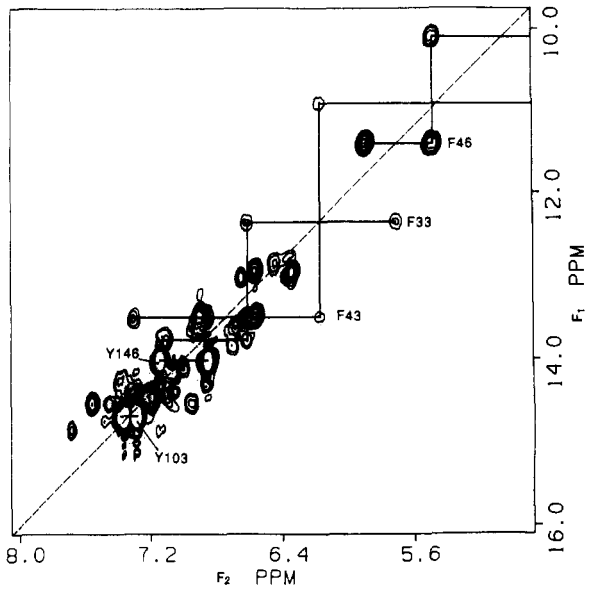

FIGURE 7: Aromatic region of the double quantum spectrum, in magnitude-mode display, of elephant MbCO, acquired with $2\tau = 40$ ms. The assignments are shown with the one-letter code for the amino acid residues. The sloping broken line represents the double quantum pseudodiagonal ($F_1 = 2F_2$). The chemical shift of the $C_\zeta H$ of Phe CD4 was calculated from $F_{1(\zeta+\epsilon)} - F_{2(\epsilon)}$. The residual water resonance was not saturated in the experiment.

system (Phe^X) with chemical shifts of 5.91, 5.49, and 4.59 ppm and another system (Phe^Y) with chemical shifts of 7.13, 6.62, and 5.71 ppm. These spin systems can be clearly verified by the phase-sensitive relayed coherence transfer spectrum (Figure 6) and the double quantum spectrum (Figure 7). The third Phe spin system (Phe^Z) has two resolved ^{1}H resonances at 7.31 and 6.18 ppm as shown clearly in Figure 1A. However, the other resonance (ζ proton) is not clearly resolved in this spectrum but appears to lie close to the H_2O resonance, which has been partially saturated and where there is a strong t_1 ridge. The double quantum spectra help to remove the solvent line as well as diagonal peaks and clearly show the missing resonance for the Phe^Z at 4.75 ppm, as calculated from the double quantum frequencies (Figure 7).[2]

The chemical shifts of the three identified Phe ring spin systems are variably upfield-shifted compared to those of a normal Phe residue, indicating that a number of these protons experience strong ring current shifts from the heme. Both elephant and sperm whale Mbs possess only three Phe residues in the heme pocket, and all three are located on the distal side of the heme (B14, CD1, CD4). The ^{1}H resonances of all these Phe residues have been assigned in sperm whale MbCO (Dalvit & Wright, 1987), and the heme ring current calculations show that they are consistent with the crystal structure (Kuriyan et al., 1986). Unfortunately, the X-ray structure of elephant Mb has not yet been reported. Phe CD1 is only one out of two completely conserved residues (F8 is the other) in Hbs and Mbs and is found approximately parallel to the heme over β meso-H. Such a position of Phe CD1 in contact with β meso-H was used in the assignment of the ^{1}H resonances of sperm whale MbCO. The Phe^Z in elephant MbCO shows NOE connectivities to the heme β meso-H (Figure 3) and is then assigned to Phe CD1. Phe CD1 in elephant MbCO has chemical shifts nearly identical with those in sperm whale MbCO (Dalvit & Wright, 1987).

The crystal structure (Kuriyan et al., 1986) shows that Phe B14 is in the proximity of Leu B10 and Phe CD1. NOESY peaks between them are observed in sperm whale MbCO, as expected, and used to assign this residue (Dalvit & Wright, 1987). Such NOESY peaks are also observed in elephant MbCO between Leu B10 and Phe^Y (Figure 5) and between Phe CD1 and Phe^Y (Figure 2), thus assigning Phe^Y to Phe B14. The interresidue NOE connectivities among Phe^Y (B14), Phe^Z (CD1), and Leu B10 demonstrate clearly that these residues are all located on the same (distal) side of the heme.

The remaining Phe^X spin system shows NOE connectivity to Phe B14 (Figure 2), which indicates that this residue is also on the distal side of the heme. Accepting that the available amino acid sequence is accurate, the present NMR data require the assignment of Phe^X to Phe CD4. NOE connectivities are not observed between the Phe CD4 ring protons and the heme substitutents. However, *strong NOESY cross peaks between Phe^X (CD4) and Leu B10 and between Phe^X (CD4) and Val E11 are observed in elephant MbCO (Figure 5), which are not seen in sperm whale MbCO.* The Phe^X (CD4) in elephant MbCO also has significantly more upfield-shifted resonances by 0.83, 1.03, and 1.97 ppm for the C_δHs, C_ϵHs, and C_ζH, respectively, when compared to sperm whale MbCO (Dalvit & Wright, 1987). Such large changes in the ring current shifts and NOE connectivities for Phe CD4 dictate a significantly altered reorientation of this residue in elephant relative to sperm whale MbCO.[3]

Discussion

Insertion of Phe CD4 into the Heme Pocket. In order to assess the orientation of Phe CD4 in elephant MbCO, the other residues in the distal heme pocket are compared first with those in sperm whale MbCO (Mabbutt & Wright, 1985; Dalvit & Wright, 1987). The highly conserved Phe CD1 is found with essentially identical chemical shifts (the differences are <0.1 ppm) and NOE connectivities to the heme as in sperm whale MbCO. Val E11 is found to have slightly smaller ring current shifts by 0.33, 0.57, 0.25, and 0.03 ppm for the γ_2 CH_3, γ_1 CH_3, β CH, and α CH, respectively, as compared to those in sperm whale MbCO. The observed NOE patterns to the heme for this residue are the same as those in sperm whale MbCO. Thus these data indicate that Val E11 is similarly oriented but possibly slightly further (~0.1 Å) away from the heme center in elephant relative to sperm whale MbCO. The side chain of Leu B10 is found to have slightly more upfield shifts by 0.16 ppm for δ_1 CH_3 and 0.18 ppm for γ CH but less upfield shift by 0.61 ppm for δ_2 CH_3, which reflects a slight rotation with respect to the heme plane (δ_1 CH_3 and γ CH closer and δ_2 CH_3 further away). The Phe B14 is suggested to slightly tilt away from the heme center, as reflected by smaller ring current shifts by 0.12, 0.17, and 0.49 ppm for the C_δHs, C_ϵHs, and C_ζH, respectively. The changes in chemical shifts for these distal residues could also be interpreted to be caused by the perturbed environment of Phe CD4. However,

[2] In addition to the aromatic spin systems of the three Phe residues, two Tyr ring spin systems in elephant MbCO (Figure 7) are identified on the basis of strong intensities in the double quantum spectrum for the pair of protons (C_δHs and C_ϵHs) (Boyd et al., 1983): Tyr^X at 7.28 and 7.38 ppm and Tyr^Y at 6.85 and 7.15 ppm. There are only two Tyr residues in elephant Mb: Tyr 103 (G4) and Tyr 146 (H23). On the basis of the similarity of these chemical shifts to those in sperm whale MbCO (Dalvit & Wright, 1987), the Tyr^X is assigned to Tyr 103 (G4) and Tyr^Y to Tyr 146 (H23).

[3] We considered the alternative assignment of Phe^X to Phe B14 but must reject it as unreasonable, since Phe B14 is anchored on the B helix on the opposite heme edge to Val E11 and since Phe B14's NOE connectivities to Val E11 and large heme-induced ring current shifts require gross conformational changes for the whole protein. Thus, the assignments of Phe^X to Phe CD4 and Phe^Y to Phe B14 are unequivocal.

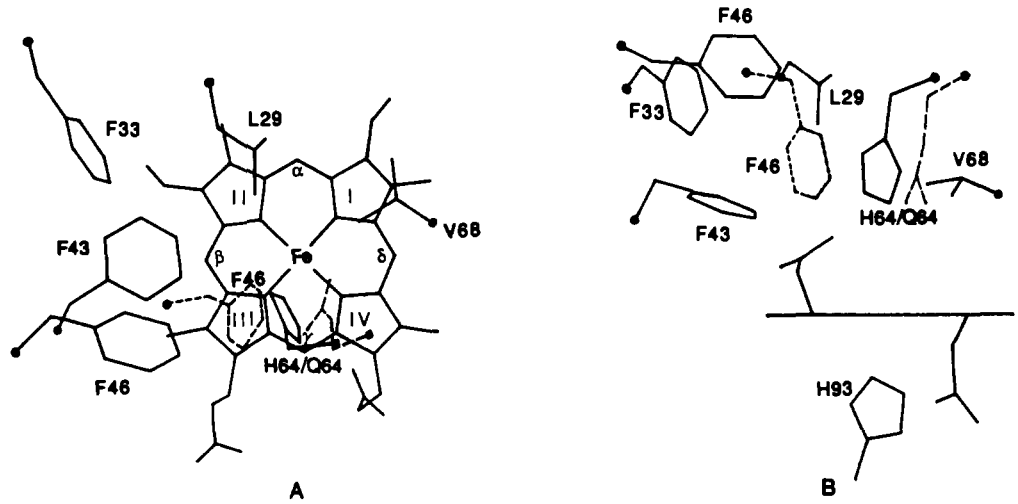

FIGURE 8: Selected residues (solid lines) in the distal heme pocket based on the X-ray structure of sperm whale MbCO (Kuriyan et al., 1986): (A) face-on view; (B) edge-on view. The dashed lines show the estimated positions of the inserted Phe CD4 and the distal E7 (64) substituted Gln in elephant Mb. The black dots indicate the positions of the C_α atoms.

the small amplitude of changes in shifts clearly shows that these residues in the distal heme pocket of elephant MbCO are minimally perturbed relative to those in sperm whale MbCO.

Thus, the orientation of Phe CD4 in elephant MbCO can initially be evaluated qualitatively by assuming that the other distal residues occupy the same positions as in the crystal structure of sperm whale MbCO (Kuriyan et al., 1986). The C_ϵHs and C_ζH of Phe CD4 in sperm whale MbCO are 6.5 and 9.8 Å (for the two C_ϵHs) and 7.5 Å (for the C_ζH) away from Val E11 γ_2 CH_3, and the C_δHs are 7.6 and 5.6 Å away from Leu B10 δ_1 CH_3; and consistent with expectation, no such NOESY peaks are observed in sperm whale MbCO (Mabbutt & Wright, 1985; Dalvit & Wright, 1987). However, strong NOESY peaks between these pairs of protons are observed in elephant MbCO (Figure 5), indicating that they are separated by <4 Å. In addition, the C_δHs of Phe CD4 also show NOE connectivities to Phe B14 C_δHs and C_ϵHs (Figure 2). Most importantly, the Phe CD4 in elephant MbCO is significantly further upfield shifted by 0.83, 1.03, and 1.97 ppm for the C_δHs, C_ϵHs, and C_ζH, respectively, when compared to those in sperm whale MbCO. The much larger ring current shifts for Phe CD4 and these newly observed NOE connectivities in elephant MbCO dictate that this residue has moved significantly closer to the heme center than that in sperm whale MbCO. The network of the newly observed NOE connectivities places the Phe CD4 ring over the pyrrole III with its C_ζH moved ~4 Å toward the iron relative to its position in sperm whale MbCO (Figure 8). Heme ring current calculations with graphic modeling of the crystal structure of sperm whale MbCO (Cross & Wright, 1985) further indicate that the Phe CD4 ring is approximately perpendicular to, and its C_ζH ~4.5 Å away from, the heme plane (Figure 8). A distance of ~5 Å from the C_ζH of Phe CD4 to the iron obtained from this qualitative ring current/NOE analysis agrees with that of 4.6 Å based on the paramagnetic relaxation measurements of the ^{1}H NMR studies of elephant metMbCN (Emerson, 1989). The similar NOEs between the Phe CD4 ring protons and the methyl groups of Leu B10 and Val E11 in elephant Mb and between the E7 His C_δH and the same methyl groups in sperm whale Mb (Dalvit & Wright, 1987) further support the new location of Phe CD4 in elephant Mb. This positioning of the Phe CD4 aromatic ring will put it in van der Waals contact with the bound CO. Thus, both ring current calculations and NOE connectivities find the insertion of Phe CD4 into the heme pocket in elephant MbCO. It is clear that the X-ray crystal structure of elephant MbCO would be very illuminating.

Elephant MbO_2 Complex. In order to examine whether the Phe CD4 insertion found in elephant MbCO also exists in the MbO_2 complex, ^{1}H NMR investigations are extended to this functionally relevant but seldom studied species. The MbO_2 complex is not very stable and subjected to autoxidation, which converts the diamagnetic MbO_2 into the paramagnetic metaquo-Mb. This problem is especially severe for 2D experiments, which require very extended data accumulation times. Elephant MbO_2, however, is well-known for its low autoxidation rate (Romero-Herrera et al., 1981), which significantly reduces but does not eliminate this problem.[4]

The DQF-COSY spectrum for the elephant MbO_2 complex is shown in Figure 1B. It is clear that the patterns of the cross peaks are similar to those of MbCO (Figure 1A), with the chemical shifts for Phe B14 at 7.18, 6.76, and 5.85 ppm and those for Phe CD4 at 5.99, 5.79, and 4.77 ppm for the C_δHs, C_ϵHs, and C_ζH, respectively. The 2-vinyl group resonates at 8.34 ppm for the H_α, 5.69 ppm for the H_{β_t}, and 5.61 ppm for the H_{β_c}, and the 4-vinyl group resonates at 8.52 ppm for the H_α, 6.44 ppm for the H_{β_t}, and 6.20 ppm for the H_{β_c}. The cross peaks for the Phe CD1 ring are not resolved at this temperature because of the line broadening resulting from the slow reorientation of the aromatic ring, as observed in sperm whale metMbCN (Emerson et al., 1988). The reorientation rate of the Phe CD1 in elephant metMbCN is even slower than that in sperm whale metMbCN (Emerson, 1989). The assignments of Phe B14, Phe CD4, and the vinyl groups in this MbO_2 complex are confirmed by the same NOE connectivities (not shown) as observed in the MbCO complex. The assigned ^{1}H resonances of the heme and amino acid residues in the elephant MbO_2 complex are included in Table I.

Thus, it is concluded that all three liganded complexes of elephant Mb, MbO_2, MbCO, and metMbCN insert the aromatic side chain of Phe CD4 into the heme pocket in a similar manner. While the E7 Gln is not yet assigned in MbCO and

[4] Since the autoxidation rate is known to be very dependent on temperature, having a larger Q_{10} value of ~5 (Brown & Mebine, 1969; Livingston et al., 1986), we recorded spectra of the MbO_2 sample at a lower temperature of 22 °C under the optimized pH and ionic strength conditions (Livingston et al., 1986; Suzuki 1987). NMR spectra after 2D experiments reveal negligible autoxidation (<5%) during 2D data acquisition.

MbO_2 from the current 2D NMR studies, the ^1H NMR studies of elephant metMbCN and metMb indicate that the distal substituted E7 Gln remains in the heme pocket and exhibits the same type of hydrogen bonding via the amide $N_\epsilon H$ proton to the coordinated ligands as found for the distal E7 His imidazole $N_\epsilon H$ in sperm whale Mb (Krishnamoorthi et al., 1984a,b), although the distal Gln in elephant Mb is probably slightly moved toward heme pyrrole IV as a result of the insertion of Phe CD4, which allows dipolar contacts between Val E11 and Phe CD4 (Figure 8). The resonance Raman study of elephant and sperm whale MbO_2 also supports the presence of E7 Gln in the heme pocket (Kerr et al., 1985).

Protein modeling on a graphics station (IRIS computer) indicates that the positioning of the aromatic ring of Phe CD4 into the heme pocket cannot be accounted for by a simple rotation of the side chain. The position of the aromatic ring relative to the heme and other residues dictates that the CD4 C_α must be moved closer to the heme by a minimum of 3 Å in elephant Mb relative to sperm whale Mb (Figure 8); and in turn, the E helix likely moves slightly away from the heme. The available experimental data on the structural and dynamic properties of Mbs have consistently showed that the CD corner is one of the most flexible portions of the backbones (Phillips, 1980; Hanson & Schoenborn, 1981; Kuriyan et al., 1986; Frauenfelder et al., 1987). Molecular dynamics simulations also demonstrate that there are large internal structural fluctuations (~2.5 Å) in the CD corner and that the C, D, and E helices have large translational rearrangements that are correlated with the flexibility of the CD loop (Elber & Karplus, 1987). Thus, the insertion of Phe CD4 and the movement of the CD corner in elephant relative to sperm whale Mb, as concluded from this study, are consistent with the other experimental data and theoretical calculations. Surprising is the fact that such a large range of structural variation in the CD corner can be induced by so few changes in amino acid residues.

Interpretation of the Functional Properties. A simple E7 His → Gln substitution is expected to lead to less steric crowding [His, 153 Å^3; Gln, 143 Å^3 (Zamyatnin, 1972)] and a minor change in polarity in the physiological pH range. The insertion of a Phe into the heme pocket accompanying the E7 His → Gln substitution in elephant Mb clearly leads to a distal pocket that is both more crowded and hydrophobic. This conclusion is independent on whether or not the inserted Phe is CD4. The increased steric crowding is consistent with the results from resonance Raman study (Kerr et al., 1985). The increase in distal pocket hydrophobicity destabilizes ferric relative to ferrous Mb, leading to the greater redox potential and the lower pK_a value of the acid–alkaline transition of the elephant Mb (Bartnicki et al., 1983). The increased distal steric crowding and hydrophobicity also serve to reduce the access of ions to the distal cavity, which is shown to be a key factor for autoxidation (Wallace et al., 1982; Springer et al., 1989), and hence accounts for a significantly lower autoxidation rate for elephant Mb relative to sperm whale Mb (by a factor of ~9 at pH 7.0) (Romero-Herrera et al., 1981; Suzuki, 1987).

Elephant Mb has similar kinetic properties for the binding of O_2 ligand and similar CO combination rate constants but decreased CO dissociation rate constants when compared to sperm whale Mb (Romero-Herrera et al., 1981; Goss et al., 1982; Mims et al., 1983; Sharma et al., 1987). These data suggest that O_2 ligand binding involves predominantly hydrogen-bonding interaction through the distal E7 residue, as observed in the crystal structures (Phillips & Schoenborn, 1981; Nagai et al., 1987). In contrast, the binding of CO ligand is predominantly involved in hydrophobic interactions (Mims et al., 1983). The altered CO dissociation constant would be consistent with the new interactions of CO ligand with the inserted Phe CD4.

Therefore, this study clearly indicates that the one-to-one interpretation of substitution of an amino acid residue (i.e., E7 His) by another (i.e., Gln) is oversimplified and that significant conformational changes of the perturbed proteins may have to be considered for interpretation of the altered functional properties.

The insertion of Phe CD4 into the distal pocket is unprecedented in structurally characterized Mbs and Hbs. The questions that remain unanswered are: Why does Phe CD4 insert into the heme pocket in elephant Mb? How many amino acid residue substitutions, relative to the reference protein sperm whale Mb, are required to induce such a structural change? The simplest substitution, E7 His → Gln, in sperm whale Mb is accessible (Springer et al., 1989; Lambright et al., 1989; Varadarajan et al., 1989). The preliminary data on sperm whale Mb mutant (E7 His → Gln) indicate a normal Phe CD4 environment (L. P. Yu, G. N. La Mar, M. Chiu, and S. A. Sligar, unpublished results) and suggest that the unusual properties of elephant Mb must result from the double substitution E7 His → Gln and CD3 Arg → Lys, although more complicated combinations with synergistically interacting surface positions may be responsible. The present results may provide incentives for further research directions on the X-ray crystallography, molecular dynamic simulations, and genetic engineering of Mbs. More detailed characterization of the solution structure of elephant Mb will require more extensive sequence-specific assignments by 2D ^1H NMR methods, and such sutides are in progress.

ACKNOWLEDGMENTS

We are grateful to S. D. Emerson for providing unpublished results on elephant metMbCN and to J. S. de Ropp and S. W. Unger of the UCD NMR facility for useful discussions.

Registry No. His, 71-00-1; Gln, 56-85-9.

REFERENCES

Baldwin, J. M. (1980) *J. Mol. Biol. 136*, 103–128.
Bartnicki, D. E., Mizukami, H., & Romero-Herrera, A. E. (1983) *J. Biol. Chem. 258*, 1599–1602.
Boyd, J., Dobson, C. M., & Redfield, C. (1983) *J. Magn. Reson. 55*, 170–176.
Brown, W. D., & Mebine, L. B. (1969) *J. Biol. Chem. 244*, 6696–6701.
Case, D. A., & Karplus, M. (1979) *J. Mol. Biol. 132*, 343–368.
Cooke, R. M., Dalvit, C., Narula, S. S., & Wright, P. E. (1987) *Eur. J. Biochem. 166*, 399–408.
Cross, K. J., & Wright, P. E. (1985) *J. Magn. Reson. 64*, 220–231.
Cutnell, J. D., La Mar, G. N., & Kong, S. B. (1981) *J. Am. Chem. Soc. 103*, 3567–3572.
Dalvit, C., & Wright, P. E. (1987) *J. Mol. Biol. 194*, 313–327.
Dene, H., Goodman, M., & Romero-Herrera, A. E. (1980) *Proc. R. Soc. London, B 207*, 111–127.
Di Iorio, E. E., Meier, U. T., Smit, J. D. G., & Winterhalter, K. H. (1985) *J. Biol. Chem. 260*, 2160–2164.
Edwards, M. W., & Bax, A. (1986) *J. Am. Chem. Soc. 108*, 918–923.
Eich, G., Bodenhausen, G., & Ernst, R. R. (1982) *J. Am. Chem. Soc. 104*, 3731–3732.

Elber, R., & Karplus, M. (1987) *Science 235*, 318–321.
Emerson, S. D. (1989) Ph.D. Thesis, University of California, Davis.
Emerson, S. D., Lecomte, J. T. J., & La Mar, G. N. (1988) *J. Am. Chem. Soc. 110*, 4176–4182.
Frauenfelder, H., Hartmann, H., Karplus, M., Kuntz, I. D., Jr., Kuriyan, J., Parak, F., Petsko, G. A., Ringe, D., Tilton, R. F., Jr., Connolly, M. L., & Max, N. (1987) *Biochemistry 26*, 254–261.
Gersonde, K., Yu, N.-T., Kerr, E. A., Smith, K. M., & Parish, D. W. (1987) *J. Mol. Biol. 194*, 545–556.
Goss, D. J., La Gow, J. B., & Parkhurst, L. J. (1982) *Comp. Biochem. Physiol. 71B*, 229–233.
Hanson, J. C., & Schoenborn, B. P. (1981) *J. Mol. Biol. 153*, 117–146.
Kerr, E. A., Yu, N.-T., Bartnicki, D. E., & Mizukami, H. (1985) *J. Biol. Chem. 260*, 8360–8365.
Krishnamoorthi, R., La Mar, G. N., Mizukami, H., & Romero, A. (1984a) *J. Biol. Chem. 259*, 265–270.
Krishnamoorthi, R., La Mar, G. N., Mizukami, H., & Romero, A. (1984b) *J. Biol. Chem. 259*, 8826–8831.
Kuriyan, J., Wilz, S., Karplus, M., & Petsko, G. A. (1986) *J. Mol. Biol. 192*, 133–154.
Lambright, D. G., Balasubramanian, S., & Boxer, S. G. (1989) *J. Mol. Biol. 207*, 289–299.
Lavalette, D., Tetreau, C., Mispelter, J., Momenteau, M., & Lhoste, J.-M. (1984) *Eur. J. Biochem. 145*, 555–565.
Li, X. Y., & Spiro, T. G. (1988) *J. Am. Chem. Soc. 110*, 6024–6033.
Liljeqvist, G., Paleus, S., & Braunitzer, G. (1982) *J. Mol. Evol. 18*, 102–108.
Livingston, D. J., Watts, D. A., & Brown, W. D. (1986) *Arch. Biochem. Biophys. 249*, 106–115.
Mabbutt, B. C., & Wright, P. E. (1985) *Biochim. Biophys. Acta 832*, 175–185.
Magde, D., Martin, J.-L., Wilson, K. R., & Dupuy, C. (1985) *Ultrashort Pulse Spectrosc. Applications 533*, 2–7.
Mims, M. P., Porras, A. G., Olson, J. S., Noble, R. W., & Peterson, J. A. (1983) *J. Biol. Chem. 258*, 14219–14232.
Muller, N., Ernst, R. R., & Wuthrich, K. (1986) *J. Am. Chem. Soc. 108*, 6482–6492.
Nagai, K., Luisi, B., Shih, D., Miyazaki, G., Imai, K., Poyart, C., De Young, A., Kwiatkowsky, L., Noble, R. W., Lin, S.-H., & Yu, N.-T. (1987) *Nature (London) 329*, 858–860.
Olson, J. S., Mathews, A. J., Rohlfs, R. J., Springer, B. A., Egeberg, K. D., Sligar, S. G., Tame, J., Renaud, J.-P., & Nagai, K. (1988) *Nature (London) 366*, 265–266.
Perutz, M. F. (1989) *Trends Biochem. Sci. 14*, 42–44.
Peyton, D. H., La Mar, G. N., Pande, U., Ascoli, F., Smith, K. M., Pandey, R. K., Parish, D. W., Bolognesi, M., & Brunori, M. (1989) *Biochemistry 28*, 4880–4887.
Phillips, S. E. V. (1980) *J. Mol. Biol. 142*, 531–554.
Phillips, S. E. V., & Schoenborn, B. P. (1981) *Nature (London) 292*, 81–82.
Romero-Herrera, A. E., Goodman, M., Dene, H., Bartnicki, D. E., & Mizukami, H. (1981) *J. Mol. Evol. 17*, 140–147.
Satterlee, J. D., Teintze, M., & Richards, J. H. (1978) *Biochemistry 17*, 1456–1462.
Sharma, V. S., John, M. E., & Waterman, M. R. (1982) *J. Biol. Chem. 257*, 11887–11892.
Sharma, V. S., Traylor, T. G., Gardiner, R., & Mizukami, H. (1987) *Biochemistry 26*, 3837–3843.
Springer, B. A., Egeberg, K. D., Sligar, S. G., Rohlfs, R. J., Mathews, A. J., & Olson, J. S. (1989) *J. Biol. Chem. 264*, 3057–3060.
States, D. J., Haberkorn, R. A., & Reuben, D. J. (1982) *J. Magn. Reson. 48*, 286–292.
Steigemann, W., & Weber, E. (1979) *J. Mol. Biol. 127*, 309–338.
Suzuki, T. (1987) *Biochim. Biophys. Acta 914*, 170–176.
Suzuki, T., & Furukohri, T. (1988) *Mem. Fac. Sci., Kochi Univ., Ser. D 9*, 13–19.
Suzuki, T., Muramatsu, R., Kisamori, T., & Furukohri, T. (1988) *Zool. Sci. 5*, 69–76.
Suzuki, T., Takagi, T., & Ohta, S. (1989) *Biochem. J. 260*, 177–182.
Tucker, P. W., Phillips, S. E. V., Perutz, M. F., Houtchens, R., & Caughey, W. S. (1978) *Proc. Natl. Acad. Sci. U.S.A. 75*, 1076–1080.
Varadarajan, R., Lambright, D. G., & Boxer, S. G. (1989) *Biochemistry 28*, 3771–3781.
Wagner, G. (1983) *J. Magn. Reson. 55*, 151–156.
Wallace, W. J., Houtchens, R. A., Maxwell, J. C., & Caughey, W. S. (1982) *J. Biol. Chem. 257*, 4966–4977.
Zamyatnin, A. A. (1972) *Prog. Biophys. Mol. Biol. 24*, 107–123.